ratio but major changes in the relative intensities of the (100), (200), and (300) reflections, which suggests a different space group (11). The observed unit cell parameters at 7.9 GPa are $a = 5.305$ (2), $c = 8.633$ (6) Å, and $V = 210.4$ (3) Å^3. A stoichiometry of 1:1 CH$_4$:H$_2$ yields a much larger volume of mixing (12%). The observed cell parameters and c/a ratio are consistent with the wurzite structure (B4) for this compound. The spectroscopic signature of this transition is the positive shift of the Q$_1$(J) hydrogen vibron with respect to the one in the pure solid at this pressure (Fig. 2B). Raman measurements of the H$_2$ vibron from this phase up to 30 GPa showed no changes, indicating that the compound is stable to at least 30 GPa (12).

The methane-rich compound (CH$_4$)$_2$H$_2$ crystallizes as a needle-shaped crystal (Fig. 2C). X-ray data were collected on a single crystal grown from a starting composition of 40% H$_2$ at 5.6 GPa. The unit cell was bct (space group I4/mcm) with $a = 7.231$ (1), $c = 5.934$ (1) Å and $V = 310.3$ (1) Å^3, for $Z = 4$. This structure is similar to the Al$_2$Cu-type structure (13), with the CH$_4$ molecules occupying the Al sites and the H$_2$ molecules occupying the Cu sites (Fig. 3B). Based on simple considerations of hard sphere packing, this is not surprising because the Al$_2$Cu family of alloys has a similar atomic (molecular) diameter ratio in the range 1.13:1 to 1.61:1. For compositions above 35% H$_2$, methane froze first; and above the peritectic pressure of 4.5 GPa, the compound (CH$_4$)$_2$H$_2$ formed through the peritectic reaction CH$_4$ (S) + L → CH$_4$ (S) + (CH$_4$)$_2$H$_2$ (S). With a composition of 20% H$_2$, the soft (CH$_4$)$_2$H$_2$ medium provided a quasi-hydrostatic environment in which to study the phase transitions in pure methane (Fig. 2D).

Compared to other binary systems such as Ar-H$_2$ (14) and He-Ne (15), in which only one compound has been observed, four solid phases have been documented here. Two of the stoichiometric solids observed fall close to the compounds observed in the N$_2$-CH$_4$ system (16). However, in contrast to that system, no unmixing was observed in the fluid phase. This comparison reveals a number of systematics in the structures of these new compounds. The formation of these van der Waals (molecular) compounds is essentially dictated by the efficient packing of hard spheres (17) used to rationalize the structures of metallic alloys. For CH$_4$(H$_2$)$_2$, the structure is similar to that of Ar(H$_2$)$_2$ (14), as is expected because the diameter ratios are fairly close to 1.22:1, which satisfies the condition for the formation of a MgZn$_2$ (Laves phase) structure (7).

REFERENCES AND NOTES

1. P. Loubeyre, in *Molecular Systems under High Pressure*, R. Pucci and G. Piccitto, Eds. (Elsevier, Amsterdam, Netherlands, 1991), pp. 245–262; J. A.
Schouten, *J. Phys. Condens. Matter* **7**, 469 (1995).
2. H. K. Mao and R. J. Hemley, *Rev. Mod. Phys.* **66**, 671 (1994).
3. J. H. van der Waals, *Ann. N.Y. Acad. Sci.* **715**, 29 (1994).
4. W. L. Vos et al., *Nature* **358**, 46 (1992).
5. R. J. Hemley et al., *Phys. Rev. B* **42**, 6458 (1990).
6. R. M. Hazen, H. K. Mao, L. W. Finger, P. M. Bell, *Appl. Phys. Lett.* **37**, 288 (1980).
7. W. Hume-Rothery, S. E. Smallman, C. W. Haworth, *The Structure of Metals and Alloys* (Institute of Metals and Alloys, London, 1969).
8. W. L. Vos, L. W. Finger, R. J. Hemley, H. K. Mao, *Phys. Rev. Lett.* **71**, 3150 (1993).
9. D. Londono, W. F. Kuhs, J. L. Finney, *Nature* **332**, 141 (1988).
10. Normalized with respect to the gas phase scattering strengths of the C–H ν_3(A$_1$) mode at 2914 cm^{-1} and the H–H Q$_1$(J) mode at 4156 cm^{-1}.
11. M. S. Somayazulu, R. J. Hemley, L. W. Finger, H. K. Mao, in preparation.
12. M. S. Somayazulu, A. F. Goncharov, R. J. Hemley, H. K. Mao, L. W. Finger, *Bull. Am. Phys. Soc.*, in press.
13. E. E. Havinga, H. Damsma, P. Hokkeling, *J. Less Common Met.* **27**, 169 (1972).
14. P. Loubeyre, R. LeToullec, J.-P. Pinceaux, *Phys. Rev. Lett.* **72**, 1360 (1994).
15. P. Loubeyre, M. Jean-Louis, R. LeToullec, L. Charon-Gerard, *ibid.* **70**, 178 (1993).
16. J. A. Schouten, M. G. E. von Hinsberg, M. I. M. Scheerboom, J. P. J. Michels, *J. Phys. Condens. Matter* **6**, A187 (1994).
17. M. D. Elkridge, P. A. Madden, D. Frenkel, *Nature* **365**, 35 (1993).

Comparison of Radiative and Physiological Effects of Doubled Atmospheric CO$_2$ on Climate

P. J. Sellers, L. Bounoua, G. J. Collatz, D. A. Randall, D. A. Dazlich, S. O. Los, J. A. Berry, I. Fung, C. J. Tucker, C. B. Field, T. G. Jensen

The physiological response of terrestrial vegetation when directly exposed to an increase in atmospheric carbon dioxide (CO$_2$) concentration could result in warming over the continents in addition to that due to the conventional CO$_2$ "greenhouse effect." Results from a coupled biosphere-atmosphere model (SiB2-GCM) indicate that, for doubled CO$_2$ conditions, evapotranspiration will drop and air temperature will increase over the tropical continents, amplifying the changes resulting from atmospheric radiative effects. The range of responses in surface air temperature and terrestrial carbon uptake due to increased CO$_2$ are projected to be inversely related in the tropics year-round and inversely related during the growing season elsewhere.

A number of simulation studies have investigated the impact of increasing atmospheric CO$_2$ concentration on the energy balance, precipitation, and surface air temperature of the Earth. A recent assessment of the results produced by different atmospheric general circulation models (AGCMs) indicates that the globally averaged surface air temperature could increase by 1.5° to 4.5°C in response to a doubling of atmospheric CO$_2$ (1). In almost all cases, the impacts of increasing CO$_2$ are conventionally associated with changes in the radiation and energy balances; physiologically induced effects on climate are ignored. In this report we investigate the potential for additional warming over the

P. J. Sellers, G. J. Collatz, S. O. Los, C. J. Tucker, National Aeronautics and Space Administration, Goddard Space Flight Center (NASA GSFC), Biospheric Sciences, Code 923, Greenbelt, MD 20771, USA.
L. Bounoua, Universities Space Research Association, NASA GSFC, Biospheric Sciences, Code 923, Greenbelt, MD 20771, USA.
D. A. Randall, D. A. Dazlich, T. G. Jensen, Department of Atmospheric Sciences, Colorado State University, Fort Collins, CO 80523, USA.
J. A. Berry and C. B. Field, Department of Plant Biology, Carnegie Institution of Washington, Stanford, CA 94305, USA.
I. Fung, Department of Earth and Ocean Sciences, University of Victoria, Victoria, British Columbia, V8N 3X3, Canada.

continents as a result of the physiological response of terrestrial vegetation when exposed to an equilibrium doubling in atmospheric CO$_2$ concentration.

Terrestrial vegetation takes up CO$_2$ for photosynthesis through small pores in the leaf surfaces called stomates. At the same time, water vapor from the leaf interior diffuses out through the stomates to the atmosphere (transpiration). Plants continuously adjust the widths of their stomatal apertures, apparently to enhance CO$_2$ uptake for a given evaporative loss of leaf water (2). Leaf stomatal conductance to water vapor transfer appears to be sensitive to variations in net photosynthetic rate, and hence to light intensity, temperature, soil moisture, and atmospheric CO$_2$ concentration, as well as to changes in humidity and CO$_2$ concentration at the leaf surface. Leaf-scale models of net photosynthetic assimilation, A, and stomatal conductance, g$_s$, have been formulated to describe these relations [see, for example, (3)].

The physiological effects on climate caused by increasing atmospheric CO$_2$ result from the dependence of photosynthesis and stomatal conductance on CO$_2$ partial pressure (Fig. 1). Short-term exposure of C$_3$ plants to 2 × CO$_2$ (a doubling of the CO$_2$

concentration) stimulates photosynthesis (Fig. 1, a and b) and decreases stomatal conductance (Fig. 1c) from C (control) to P (physiological response to $2 \times CO_2$). After long-term exposure to increased atmospheric CO_2, plants may reduce their biochemical capacity for photosynthesis, V_{max}. This response is represented by PV (physiological effects due to $2 \times CO_2$ with "down-regulated" V_{max}) in Fig. 1, b and c. The PV case in Fig. 1 depicts a maximum down-regulation response in which photosynthesis at $2 \times CO_2$ is adjusted to maintain about the same rate as under normal ($1 \times CO_2$) conditions. Down-regulation has been observed in some, but not all, experiments with plants grown at elevated concentrations of CO_2 (4). The extent of down-regulation apparently depends on species, nutritional status, and environmental stresses (5). Our calculations indicate an associated decrease in stomatal conductance in the range of 25% (P) to 50% (PV), which is consistent with the range of experimental observations on trees (6) and herbaceous species (7). Analysis of stomatal densities on fossil or otherwise preserved leaf surfaces (8) also implies that g_s has decreased in response to past increases in atmospheric CO_2 partial pressure.

The lines linking the P and PV points in Fig. 1, b and c, thus describe the likely range of leaf-scale physiological responses to increased CO_2 in the absence of other climatic effects. Photosynthesis could increase significantly, with a small reduction in stomatal conductance (the P case); photosynthesis might remain more or less constant and g_s and transpiration significantly reduced (the PV case); or something in between could occur.

The improved simple biosphere model (SiB2) incorporates a coupled photosynthesis-conductance submodel into its vegetation canopy model (3, 9, 10) so that the exchanges of energy, water, and carbon between the land and atmosphere are modeled as tightly linked processes. SiB2 has been linked to an AGCM (11), which also incorporates simple ocean and sea-ice models (12). Global satellite data for 1987 were used to define the type, density, and greenness of the vegetation worldwide at monthly intervals (13). The use of these data should correct many biases in earlier survey-based descriptions; for example, overestimation of vegetation density in the boreal forest (14). The satellite data form the basis for specifying monthly fields of albedo, surface roughness, and a canopy light-use parameter that is used to scale up the leaf physiological model to the canopy scale (that is, to integrate leaf photosynthesis to canopy photosynthesis) and leaf conductance, g_s, to canopy conductance, g_c (9). The model also calculates the contributions of canopy interception loss and soil evaporation to the total evapotranspiration flux. The results from

large-scale field experiments (15) have been used to test the scaling assumptions involved in the use of area-averaged satellite data to describe the vegetation state. The combined SiB2-GCM produces plausible fields of evapotranspiration, carbon assimilation, and surface energy-balance components in addition to reasonable climate simulations (11). Simulations produced by the SiB2-GCM have been used in other biosphere-atmosphere studies (16).

We conducted model runs at 7.2° by 9.0° spatial resolution and nine layers in the ver-

Fig. 1. Leaf photosynthesis and conductance responses to local increases in atmospheric CO_2 for light-saturated conditions, based on leaf-scale model results. (a) Dependence of leaf photosynthesis for C_3 and C_4 vegetation on exterior air CO_2 concentration. (b) C_3 photosynthesis curves for unadjusted (C and P cases) and down-regulated (PV case) physiology. The down-regulated photosynthetic rate at $2 \times CO_2$ is the same as the control case ($1 \times CO_2$) photosynthetic rate. (c) Effects on stomatal conductance. Curves show the dependence of stomatal conductance with increasing CO_2 for unadjusted vegetation (P case) and down-regulated physiology (PV case).
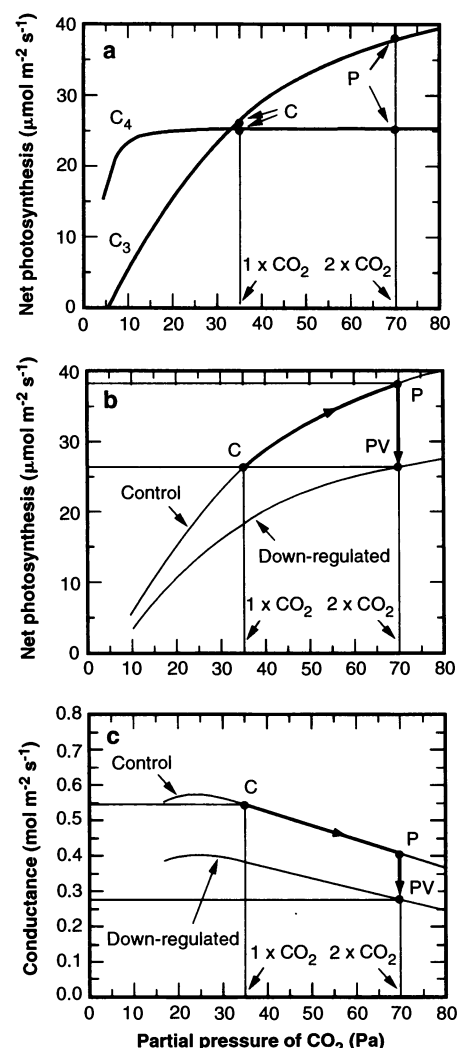
tical. First, we ran the model using observed climatological sea surface temperatures and the current $1 \times CO_2$ concentration [350 parts per million (ppm)] for 10 years to obtain the implied ocean heat transports (12, 17) and initial conditions for the experimental runs. This was followed by six 30-year integrations (runs) in which sea surface temperatures and sea ice were permitted to evolve with time (Fig. 2).

1) The control (C) run. This consisted of an integration from the initial conditions out to 30 years using $1 \times CO_2$ (350 ppm) for both the radiative transfer code in the AGCM and the vegetation physiological model.
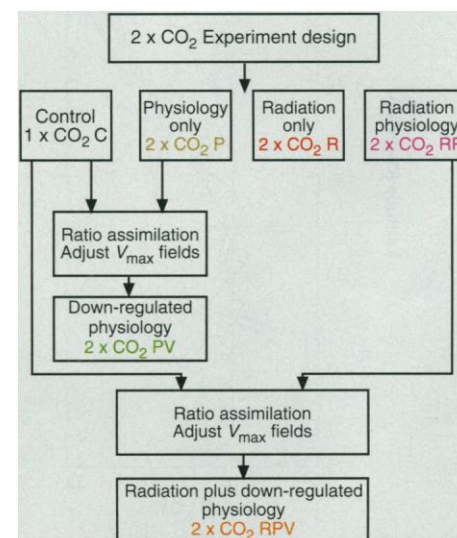
2) The physiology-only (P) run. The CO_2 concentration in the AGCM boundary layer was maintained at $2 \times CO_2$ (700 ppm) and thus directly influenced the photosynthesis-conductance model (see Fig. 1). In this run, the biome-dependent physiological parameter that limits the maximum photosynthetic rate V_{max} was the same ("unadjusted") as in the control run. The radiation code operated on a $1 \times CO_2$ (350 ppm) CO_2 atmosphere.

3) The down-regulated physiology (PV) run. The assimilation rates calculated for each grid point for the last 10 years of the C and P integrations were time-averaged and ratios were determined (C/P). These ratios were used to reduce proportionally the V_{max} values at every grid point to simulate a large down-regulation effect. The result is that, at $2 \times CO_2$, the assimilation rates calculated by the vegetation model in the PV run should approach those produced in the C case (see Fig. 1b).

4) The radiation-only (R) run. This is a conventional $2 \times CO_2$ integration in

Fig. 2. Sequence and type of numerical experiments performed with the biosphere-atmosphere model SiB2-GCM. Each case is described in the text.

which only the AGCM radiative transfer code responds to $2 \times CO_2$; the vegetation "sees" only $1 \times CO_2$.

5) The radiation plus physiology (RP) run. This is a combination of the R and P

6) The radiation plus down-regulated physiology (RPV) run. The assimilation fields of the last 10 years of the C and RP runs were averaged and their ratios were applied to the V_{max} fields in the same way as for PV. We then ran the RPV case forward using these adjusted fields and $2 \times CO_2$ values for both the AGCM radiation code and the atmospheric boundary layer in contact with the vegetation.

Table 1 shows assimilation rate (A), canopy conductance (g_c); evapotranspiration rate (E), precipitation, and surface air temperature (T) values for each run and also the changes relative to the control run.

The impact of the radiation-only (R case) treatment on assimilation (A) was very small; the assimilation fields generated in the C and R cases were almost identical

treatments; the atmospheric radiation code works with $2 \times CO_2$ as does the (unadjusted) physiology.

everywhere. The P and RP runs had significantly higher A values than did their $1 \times CO_2$ (physiology) counterparts, the C and R cases, respectively. These results were anticipated from an inspection of Fig. 1. The down-regulated A values (PV and RPV cases) are slightly increased, ~10%, over the control case (C). This difference indicates that the down-regulation of A in the PV and RPV treatments was not complete, largely because A is enhanced at elevated CO_2 concentrations in C_3 plants at lower light intensities; that is, when V_{max} is not limiting.

The overall effect of down-regulation (PV and RPV cases) was to reduce g_c values by 35% relative to the C or R cases, whereas the unadjusted physiology treatments (P and RP cases) gave reductions of ~25%. This range of responses falls within that observed in laboratory and field $2 \times CO_2$ manipulation experiments (4–7). There is little dif-
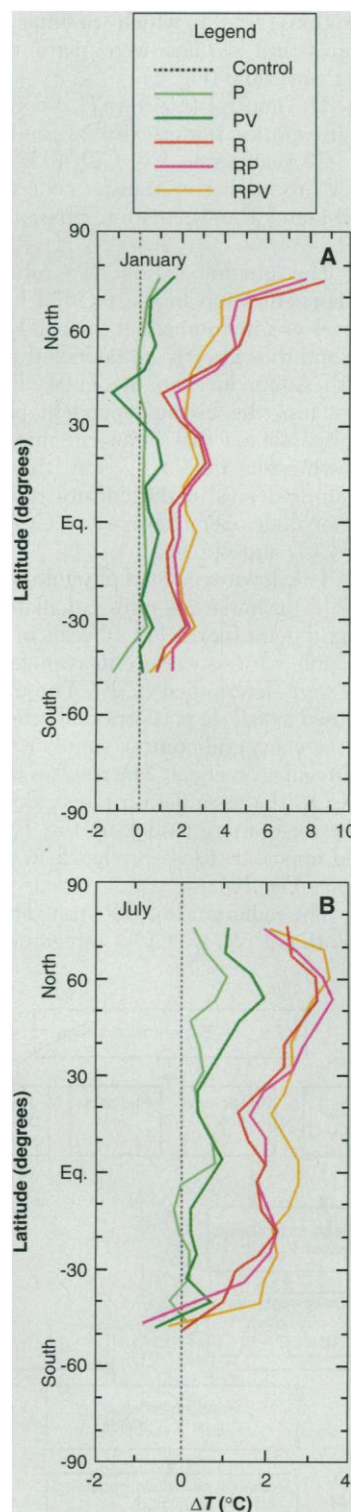
Fig. 3. Zonal mean T for the last 10 years of the simulations for all land points for the experiments discussed in the text, expressed as differences from the control ($1 \times CO_2$) case. (**A**) January; (**B**) July.

Table 1. Summary of results from the six experiments described in the text: C (control; $1 \times CO_2$ for radiation and physiology); P ($1 \times CO_2$ for radiation, $2 \times CO_2$ for physiology); PV ($1 \times CO_2$ for radiation, $2 \times CO_2$ for down-regulated physiology); R ($2 \times CO_2$ for radiation, $1 \times CO_2$ for physiology); RP ($2 \times CO_2$ for radiation, $2 \times CO_2$ for physiology); and RPV ($2 \times CO_2$ for radiation, $2 \times CO_2$ for down-regulated physiology). Values are means for the last 10 years of the 30-year simulations. Values in parentheses are the percent differences from C, except in the case of surface air temperature where the values are the differences from C. Dashes indicate not applicable.

Experiment	Assimilation ($\mu mol\ m^{-2}\ s^{-1}$)	Canopy conductance ($mm\ s^{-1}$)	Evapo-transpiration ($W\ m^{-2}$)	Precipitation ($mm\ day^{-1}$)	Surface air temperature (°C)
			Tropics (14.4°S to 14.4°N)		
C	6.04 (—)	2.79 (—)	100.8 (—)	4.36 (—)	28.1 (—)
P	7.96 (31.7)	2.06 (−26.1)	96.7 (−4.0)	4.34 (−0.4)	28.5 (0.4)
PV	6.87 (13.8)	1.82 (−34.8)	96.5 (−4.2)	4.35 (−0.2)	28.8 (0.7)
R	6.08 (0.6)	2.81 (0.6)	105.9 (5.1)	4.58 (5.0)	29.8 (1.7)
RP	8.10 (35.1)	2.12 (−24.1)	102.6 (1.9)	4.58 (5.0)	30.2 (2.1)
RPV	6.71 (11.0)	1.79 (−35.9)	100.0 (−0.8)	4.45 (2.1)	30.6 (2.6)
			Mid-latitudes (28.8°N to 50.4°N)		
C	1.77 (—)	0.79 (—)	49.6 (—)	2.70 (—)	17.4 (—)
P	2.62 (48.3)	0.61 (−23.4)	49.3 (−0.6)	2.69 (−0.2)	17.7 (0.3)
PV	1.96 (10.8)	0.49 (−38.3)	48.1 (−3.1)	2.78 (3.0)	17.9 (0.5)
R	1.72 (−2.5)	0.79 (−0.9)	52.3 (5.4)	2.91 (7.7)	20.0 (2.6)
RP	2.53 (43.4)	0.61 (−23.8)	51.5 (3.8)	2.89 (6.8)	20.3 (2.9)
RPV	2.02 (14.1)	0.51 (−35.9)	50.4 (1.6)	2.79 (3.1)	20.0 (2.6)
			North latitudes (50.4°N to 72.0°N)		
C	1.67 (—)	0.92 (—)	38.6 (—)	2.35 (—)	4.8 (—)
P	2.26 (35.6)	0.68 (−25.9)	37.7 (−2.2)	2.33 (−1.1)	5.1 (0.3)
PV	1.76 (6.0)	0.59 (−35.7)	37.0 (−4.1)	2.34 (−0.6)	5.9 (1.1)
R	1.63 (−2.0)	0.91 (−0.6)	41.2 (6.8)	2.54 (7.8)	8.8 (4.0)
RP	2.25 (35.0)	0.69 (−24.5)	39.9 (3.4)	2.49 (5.8)	8.7 (3.9)
RPV	1.81 (8.9)	0.62 (−32.4)	39.0 (1.0)	2.43 (3.4)	8.1 (3.3)
			All land points		
C	2.65 (—)	1.21 (—)	58.9 (—)	2.90 (—)	19.6 (—)
P	3.59 (35.3)	0.90 (25.1)	57.6 (−2.3)	2.89 (−0.3)	19.8 (0.3)
PV	2.93 (10.6)	0.78 (−35.2)	56.9 (−3.5)	2.94 (1.3)	20.2 (0.7)
R	2.65 (0.0)	1.21 (0.2)	62.3 (5.8)	3.10 (7.0)	22.2 (2.6)
RP	3.59 (35.5)	0.92 (−23.8)	60.9 (3.3)	3.09 (6.5)	22.4 (2.8)
RPV	2.94 (11.0)	0.79 (−34.1)	59.1 (0.3)	2.99 (3.0)	22.2 (2.7)
			Global land and ocean		
C			96.0 (—)	3.29 (—)	18.5 (—)
P			95.8 (−0.2)	3.28 (−0.2)	18.7 (0.1)
PV			96.0 (0.1)	3.29 (0.1)	18.9 (0.3)
R			100.1 (4.2)	3.43 (4.2)	20.4 (1.9)
RP			99.9 (4.0)	3.42 (4.0)	20.5 (1.9)
RPV			99.1 (3.3)	3.40 (3.3)	20.4 (1.8)

ference between the g_c values in the R and C cases, which is consistent with the A results discussed above. Canopy conductance generally decreases away from the equator, following the environmental and vegetation density gradients. We therefore expect to see the largest physiological impacts of $2 \times CO_2$ on the E rates in the tropics and smaller effects in the high latitudes.

The physiological effects of P and PV act to reduce E as the stomatal conductance falls (see Fig. 1c). However, the R runs resulted in an increase in available energy (net radiation) at the Earth's surface and, in the absence of physiological effects, E was boosted. When the physiological effects were applied along with the radiative effects, E was progressively reduced (in the RP and RPV cases) so that ultimately the global mean value of E for land in the RPV case was about the same as it was in the C case. The physiological effects thus largely counteracted the radiative effects on E in the RPV case. However, the additional available energy at the surface (net radiation) resulting from the radiative response to $2 \times CO_2$ was then released as sensible heat, causing a further increase in T in the absence of nonlocal effects.
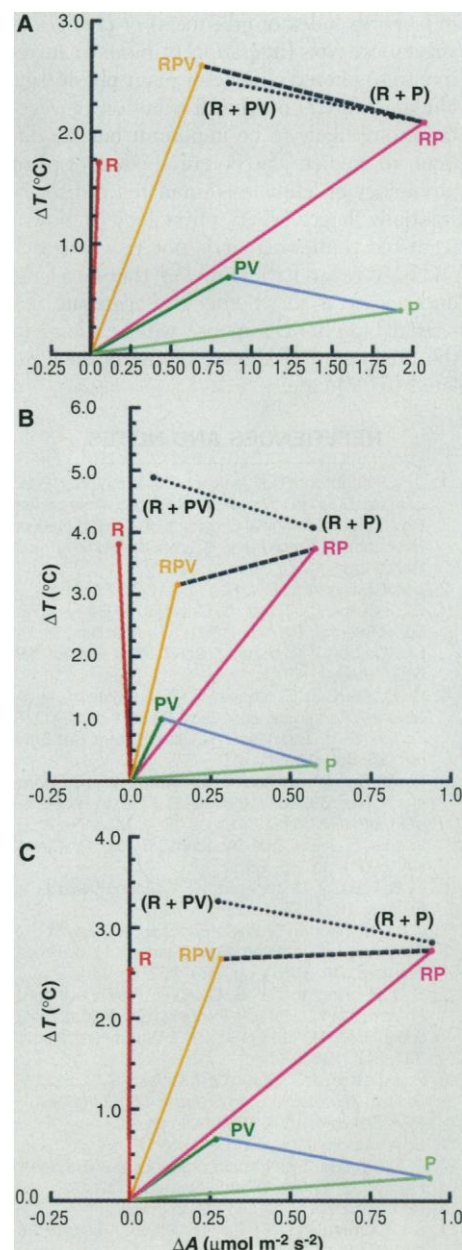
For most places, the effects of the physiological treatments (P, PV, RP, and RPV cases) on precipitation were small compared with those of radiation (R case). There were only small changes in the total land precipitation rate in the P and PV cases. However, precipitation increased significantly in the R case, in line with most other AGCM $2 \times CO_2$ studies, then fell off slightly in the RP case and was reduced further in the RPV treatment.

The regional and temporal distributions of the changes in T due to physiological effects are striking (see Fig. 3). The P and PV effects were generally small compared with those in the R runs and are consistent with the reductions in E (Table 1) and our interpretation of Fig. 1. The increase in temperature in the R run is large in the Northern Hemisphere and relatively small at lower latitudes, which is in line with results from previous "greenhouse effect" (R case) studies. In July, the RP and RPV results showed proportionally larger increases in T in the tropics, which reduced the July mean meridional temperature gradient over land in the Northern Hemisphere relative to that in the R case (Fig. 3B). Surprisingly, in January, the RP and RPV cases gave rise to a modest reduction in temperature in the land boreal zone relative to that in the R case (see Fig. 3A), which is in contrast to earlier studies (18–20). This result implies that nonlocal effects, generated by the strong year-round physiological responses in the tropics, can affect the high-latitude climate. Thus, the radiative and physiological responses to $2 \times CO_2$ combine in a nonadditive way.

The R results produced by SiB2-GCM give a warming at the low end of the range obtained from other numerical simulations of the equilibrium response to $2 \times CO_2$ (1): The total increase in global T in the R case was 1.9°C. The effects of physiological responses to $2 \times CO_2$ alone, in the absence of radiative effects, were anticipated from a simple consideration of the role of physiological processes in the surface energy budget (P and PV cases). The combination of physiological and radiative effects produced big impacts in the tropics, where physiological effects increased the R-case temperature increment from 1.7°C to between 2.1°C (RP case) and 2.6°C (RPV case). The physiologically induced effects are concentrated around midday, and so many of the effects generated by the RP and RPV warmings would be greater than those implied by the increases in mean temperatures. The projected tropical temperature increase of 2.6°C (RPV case) is comparable to the results of Amazon deforestation simulation studies, which typically yield increases of 2° to 4°C in T as a result of replacing all of the primary tropical forest with C_4 pasture. It has been suggested that such a climate change would have substantial ecological effects (21). However, a doubling of atmospheric CO_2 is more likely to occur than is the complete deforestation of the Amazon within the next century.

Figure 4 compares the changes in global A and T resulting from the different treatments; the total response to $2 \times CO_2$ should lie somewhere along the RP-RPV axes for all cases. The RP and RPV results in Fig. 4 can be compared with the sum of vectors representing the results of separate R and P, PV treatments. We have constructed analogs to the RP and RPV cases using (R + P) and (R + PV) vectors, respectively, and have plotted

Fig. 4. Changes in assimilation rate, ΔA, plotted against changes in surface temperature, ΔT, for different land areas for all the experiments described in text. All differences are defined relative to the control (1 × CO_2) case. The vectors (R) and (P, PV) show the separate effects of radiation and physiology, respectively. (**A**) Tropics, 14.4°S to 14.4°N; (**B**) northern latitudes, 50.4°N to 70°N; and (**C**) all land points. The dashed line joining the RPV and RP points is the axis linking the results of the combined radiation and physiology experiments (RPV and RP cases). The dotted line joining the "constructed" vectors (R + PV) and (R + P) is the analog of the RPV-RP axis, created by joining the points generated from the vector sums (R + PV) and (R + P). If the radiation and physiology responses were completely additive, the two axes (RPV-RP) and (R + PV)–(R + P) would lie on top of each other. This is almost true for the land tropics (A) but is obviously not true for the northern latitudes (B) or for all land points (C). This result indicates that the physiological response of the tropics may play a strong role in determining the climatic response to $2 \times CO_2$ at higher latitudes.

them on Fig. 4. A comparison of the RP with (R + P), and the RPV with (R + PV) points indicates that the interactions between the radiation and physiological effects can be nonadditive depending on geographical location; that is, the two vectors cannot be treated independently because of nonlocal influences, particularly in the northern mid- and high latitudes (Fig. 4B). In the tropics, however, the results suggest that these effects are approximately additive, presumably because local processes dominate in this zone (Fig. 4A). This result is relevant to field studies where vegetation canopies are exposed to enriched CO_2. Figure 4 implies that these studies, which generally focus on the carbon budget, should also include energy budget (radiation, water, and heat fluxes) measurements. It will be necessary to combine the results from these

studies with the anticipated changes in the energy and water balances from AGCM investigations in order for a complete picture of the total environmental response to increased CO_2 to emerge.

In the tropics, it is projected that the value of A for the terrestrial biosphere is inversely related to changes in T under 2 × CO_2 conditions (see the RPV-RP axis in Fig. 4A). For the northern latitudes, this is true for the growing season but, because of the lower winter temperatures associated with the RPV case, the mean annual A and T values appear to be correlated (Fig. 4B). For the globe, the net result is that total A varies widely for little variation in the global mean value of T (Fig. 4C).

We performed these simulations using observed vegetation conditions for 1987, as obtained from satellite data. We did not consider morphological responses (that is, changes in leaf area index or greenness) or changes in vegetation type (migration of biomes) in response to altered climate or plant physiology. Human impacts on the distribution of vegetation are likely to be important but are difficult to predict. The potential effect of plant physiology on climate is simulated to be substantially larger when physiology is down-regulated than when it is not (PV versus P and RPV versus RP). However, there is a large uncertainty as to whether the aggregate terrestrial biospheric response will be closer to the unadjusted (RP) case or the down-regulated (RPV) case.

REFERENCES AND NOTES

1. J. T. Houghton, G. J. Jenkins, J. J. Ephraums, Eds., *Climate Change: The IFCC Scientific Assessment* (World Meteorological Organization–United Nations Environment Programme, Cambridge Univ. Press, Cambridge, 1990).
2. I. R. Cowan, *Adv. Bot. Res.* **4**, 117 (1977).
3. G. J. Collatz, J. T. Ball, C. Grivet, J. A. Berry, *Agric. For. Meteorol.* **54**, 107 (1991); G. J. Collatz, M. Ribas-Carbo, J. A. Berry, *Aust. J. Plant Physiol.* **19**, 519 (1992).
4. C. B. Field, F. S. Chapin III, P. A. Matson, H. A. Mooney, *Annu. Rev. Ecol. Syst.* **23**, 201 (1992); D. T. Tissue, R. B. Thomas, B. R. Strain, *Plant Cell Environ.* **16**, 859 (1993).
5. C. A. Gunderson and S. D. Wullschleger, *Photosynth. Res.* **39**, 369 (1994); C. B. Field, in *Response of Plants to Multiple Stresses*, H. A. Mooney, W. E. Winner, E. J. Pell, Eds. (Academic Press, San Diego, CA, 1991), pp. 35–65.
6. C. B. Field, R. B. Jackson, H. A. Mooney, *Plant Cell Environ.* **18**, 1214 (1995).
7. J. I. L. Morison, in *Stomatal Function*, E. Zeiger, G. D. Farquhar, I. R. Cowan, Eds. (Stanford Univ. Press, Stanford, CA, 1987), pp. 229–252.
8. D. J. Beerling and W. G. Chaloner, *Rev. Palaeobot. Palynol.* **81**, 11 (1994); J. Penuelas and R. Matamala, *J. Exp. Bot.* **41**, 1119 (1990); F. I. Woodward, *Nature* **327**, 617 (1987).
9. P. J. Sellers, J. A. Berry, G. J. Collatz, C. B. Field, F. G. Hall, *Remote Sensing Environ.* **42**, 187 (1992).
10. P. J. Sellers *et al.*, *J. Climate*, in press.
11. D. A. Randall *et al.*, *ibid.*, in press.
12. T. G. Jensen, *Department of Atmospheric Science Paper 593*, Colorado State University (1995).
13. P. J. Sellers *et al.*, *J. Climate*, in press.
14. J. L. Dorman and P. J. Sellers, *J. Appl. Meteorol.* **28**, 833 (1989).
15. P. J. Sellers, M. D. Heiser, F. G. Hall, *J. Geophys. Res.* **97**, 19033 (1992); P. J. Sellers *et al.*, *ibid.* **100**, 25607 (1995).
16. P. Ciais, P. P. Tans, M. Trolier, J. W. C. White, R. J. Francey, *Science* **269**, 1098 (1995); A. S. Denning, I. Fung, D. A. Randall, *Nature* **376**, 240 (1995); P. Ciais *et al.*, *J. Geophys. Res.* **100**, 5051 (1995).
17. J. Hansen *et al.*, *Climate Process and Climate Sensitivity*, J. E. Hansen and T. Takahashi, Eds. (Maurice Ewing Series 5, American Geophysical Union, Washington, DC, 1984), pp. 130–163.
18. Our results are at odds with those reported in two previous studies (*19, 20*). The land surface parameterizations used in those two studies were based on highly empirical leaf stomatal conductance formulations that were not linked to photosynthetic processes. Also, the location and state of the global vegetation were based on extrapolations from a relatively small number of ground surveys reported in the ecological literature. Both studies imposed a halving (that is, a 50% reduction) of stomatal conductance everywhere, which may be compared with the reductions of between 25% (P and RP cases) and 35% (PV and RPV cases) calculated for g_c in our study. In one of the studies (*19*), evapotranspiration in the tropics was almost unaffected by physiological effects; this may be because that model distributes convective precipitation evenly over land grid squares, resulting in an over-estimation of canopy interception loss and a reduction in the importance of canopy transpiration to the total latent heat flux. Both studies projected significant impacts of physiological effects in the boreal zone in July, which led to increases in surface temperature there. For the same area, our results indicate that the combined (radiative plus physiological) responses to 2 × CO_2 yield only a slight warming relative to the R case in summer and a slight cooling in winter (Fig. 3).
19. A. Henderson-Sellers, K. McGuffie, C. Gross, *J. Climate* **8**, 1738 (1995).
20. D. Pollard and S. L. Thompson, *Global Planet. Change* **10**, 1229 (1995).
21. C. A. Nobre, P. J. Sellers, J. Shukla, *J. Climate* **4**, 957 (1991).
22. Supported by NASA Earth Observing System (EOS) funds (Sellers-Mooney Interdisciplinary Science Project). We gratefully acknowledge encouragement and support from G. Asrar and thank the NASA Center for Computational Sciences for their cooperation and L. Blasingame and V. McElroy for typing the manuscript.

The Amyloid Precursor Protein of Alzheimer's Disease in the Reduction of Copper(II) to Copper(I)

Gerd Multhaup,* Andrea Schlicksupp, Lars Hesse, Dirk Beher, Thomas Ruppert, Colin L. Masters, Konrad Beyreuther

The transition metal ion copper(II) has a critical role in chronic neurologic diseases. The amyloid precursor protein (APP) of Alzheimer's disease or a synthetic peptide representing its copper-binding site reduced bound copper(II) to copper(I). This copper ion–mediated redox reaction led to disulfide bond formation in APP, which indicated that free sulfhydryl groups of APP were involved. Neither superoxide nor hydrogen peroxide had an effect on the kinetics of copper(II) reduction. The reduction of copper(II) to copper(I) by APP involves an electron-transfer reaction and could enhance the production of hydroxyl radicals, which could then attack nearby sites. Thus, copper-mediated toxicity may contribute to neurodegeneration in Alzheimer's disease.

The major component of Alzheimer's disease (AD) amyloid βA4 is derived from the transmembrane protein APP (*1*). The central role of APP has emerged from the identification of genes that cosegregate with the disease and influence βA4 formation (*2*). The normal cellular function of APP is unknown. Work with different cell lines has shown that the secreted or membrane-associated forms of APP regulate cell growth and neurite length and participate in cell-cell and cell-matrix adhesion (*3*). APP binds to collagen, laminin, and heparan sulfate side chains of proteoglycans (*4*).

G. Multhaup, A. Schlicksupp, L. Hesse, D. Beher, K. Beyreuther, ZMBH–Center for Molecular Biology Heidelberg, University of Heidelberg, Im Neuenheimer Feld 282, D-69120 Heidelberg, Germany.
T. Ruppert, Department of Virology, University of Heidelberg, D-69120 Heidelberg, Germany.
C. L. Masters, Department of Pathology, University of Melbourne, Parkville, Victoria 3052, Australia, and Neuropathology Laboratory, Mental Health Research Institute of Victoria, Parkville, Victoria 3052, Australia.

*To whom correspondence should be addressed. E-mail: gmulthaup@sun0.urz.uni-heidelberg.de

APP isoforms (containing the Kunitz protease inhibitor domain) that form complexes with extracellular proteases are internalized by the apolipoprotein E receptor LRP (low density lipoprotein receptor–related protein) (*5*). A Zn(II)-binding site resides within APP residues 181 to 200 (*6*), and a Cu(II)-binding site resides within APP residues 135 to 155 (*6, 7*). Zn(II) and Cu(II) binding influence APP conformation, stability, and homophilic interactions (*6, 7*). In the *APP* gene family, both binding sites are conserved in *APLP2*, whereas in *APLP1* only the Zn(II) site is present (*6, 7*).

In neurons, APP is first delivered from the cell body to the axonal cell surface and then to the dendritic plasma membrane (*8*). If APP undergoes transcytosis from axons to dendrites, APP could function as a transcytotic receptor in neurons and could facilitate the transcellular transport of cerebral Zn(II) and Cu(II). Copper is an important component of various redox enzymes. Free Cu is also a toxic ion, as exemplified by its ability to inactivate proteins through ty-